Proc. Natl. Acad. Sci. USA
Vol. 85, pp. 103–106, January 1988
Biophysics

Automated laser-scanning-microbeam fluorescence/Raman image analysis of human lens with multichannel detection: Evidence for metabolic production of a green fluorophor

(fluorophor distribution/laser microprobe)

NAI-TENG YU*†, MING-ZHI CAI*, DEBORAH JUI-YUAN HO*, AND JOHN F. R. KUCK, JR.*†

*School of Chemistry, Georgia Institute of Technology, Atlanta, GA 30332; and †Department of Ophthalmology, Emory University Medical School, Atlanta, GA 30322

Communicated by J. L. Oncley, September 3, 1987 (received for review June 2, 1987)

ABSTRACT **A laser-microprobe fluorescence/Raman spectrometer with a 700-channel detector has been constructed and applied to the collection of data on the distribution of a green fluorophor throughout the exposed area of a human lens sectioned along the visual axis. The area (≈6.5 × 9.5 mm) covering the lens section was scanned automatically by the microprobe programmed to measure the fluorescence intensity at 1200 data points. The spectrometer output was accumulated in a microcomputer and displayed as a three-dimensional perspective view showing the fluorescence intensity at each point on the grid. The method permits the precise and detailed mapping at high resolution of the spatial distribution of a fluorophor or Raman-emissive constituent in a plane of the frozen lens to give results not obtainable by any other feasible procedure. The green fluorophor (441.6 nm, excitation wavelength; 520 nm, peak emission wavelength) has a distribution indicating a metabolic rather than a photochemical mode of production. Moreover, the lower level of fluorophor in the anterior segment suggests the existence of mechanisms in the anterior cortex (including the epithelium) that reduce significantly the accumulation of fluorophor. Such distribution studies are invaluable in clarifying metabolic interrelationships among the different zones of the lens, including especially photochemical reactions postulated to involve the effect of daylight on the lens in human subjects.**

The application of fluorescence and Raman spectroscopy to human and animal lenses has yielded information on the intact living lens that is hardly obtainable by other means (1, 2). We herein describe a greatly modified system that presents several advantages over our previous procedure that required the excitation beam to penetrate the lens at least to the zone where the emission originated. The system scans the surface of a frozen lens section and is, therefore, not affected by opaque regions in the body of the lens; this is a great advantage for cataract research.

Our fluorescence/Raman imaging system has a number of important capabilities: (*i*) multichannel detection of "position-defined" fluorescence/Raman spectra from gridded points (1–8 μm); (*ii*) scanning of micro (10 μm × 10 μm) and macro (2.5 cm × 2.5 cm) samples; (*iii*) automated simultaneous acquisition of intensity data of up to six spectral lines (either peak or integrated intensities) from each point; (*iv*) excellent stray-light rejection to allow detection of weak Raman lines from solid samples; (*v*) normalization of fluorescence intensity with Raman signals (fluorescence/Raman intensity ratio); and (*vi*) presentation of the *x*–*y* data set in three-dimensional perspective, three-dimensional perspective with cursor-sectioning, six-color map representing regions of various intensity intervals, and topographic contour map with lines intersecting the intensity data with constant height intensity planes.

We here describe how it has been employed to make fluorescence intensity measurements from a human lens section fitted into a slightly larger domain of 1200 data points. The 441.6-nm line of a He/Cd laser was used as an excitation source, and the concentration of a green fluorophor was monitored at 520 nm (emission maximum). This age-dependent fluorophor is present in the infant lens, in addition to the major lens fluorophor (3-hydroxy-L-kynurenine *O*-β-glucoside) that is known to be metabolically produced and characterized by an emission maximum at 440 nm when excited at 350 nm (3, 4). The lens section was made perpendicular to the equatorial plane and coincided with the optical axis so that the anterior and posterior curvatures were discernible.

Circumstantial evidence indicates that chronic exposure of human eyes to ambient near-UV radiation may cause photocatalyzed reactions that initiate the formation of nuclear senile cataract with a concomitant production of fluorescent chromophors (5–8). The examples of these reactions are the photooxidation of tryptophan (9, 10) and the generation of singlet oxygen by UV and photosensitizers endogenous to the human lens (11). However, fluorophors may also be produced by metabolic processes during aging and/or pathologic development. In the mouse lens, Yu *et al.* (12) have demonstrated that the rate of production of a blue–green fluorophor (emission maximum at 496 nm with excitation at 406.7 nm) is the same for animals reared in the dark or in the light.

The geometric distribution of a fluorophor in the human lens may give evidence for its generation by ambient light or by metabolic processes. If a lens fluorophor is generated by light, its accumulation should bear certain geometrical characteristics. Since the light strikes the anterior part of the nucleus first and is absorbed there, the fluorophor concentration should expand anteriorly but not posteriorly. The shape of the fluorophor distribution in an old lens should be asymmetric along the optical axis. Furthermore, because of the pupillary action in regulating the light allowed to enter the eye, the more intense the light, the more the light is restricted to a pathway coincident with the optical axis. Thus, viewed at the anterior pole along the optical axis, the fluorophor concentration should be higher at the center.

This paper presents the precise distribution profiles of the green fluorophor for both young (5-month-old) and old (73-year-old) lenses. Based on the distribution patterns and intensity data, we conclude that this green fluorophor is not produced by photocatalyzed reactions. It is purely a metabolic product resulting from normal lens aging.

The publication costs of this article were defrayed in part by page charge payment. This article must therefore be hereby marked "*advertisement*" in accordance with 18 U.S.C. §1734 solely to indicate this fact.

MATERIALS AND METHODS

Each human lens was placed in a rectangular cavity in an aluminum block of suitable dimension so that the optical axis was horizontal and coincident with the surface plane of the block. One-half of the lens was above the surface of the aluminum block. The lens was then frozen in the block that was transferred to a thermoelectrically cooled plate (−50°C) attached to the computer-controlled x–y translation stage. After the upper half of the lens was shaved away by a razor blade, the lower half with a flat surface was then covered by a layer of glycerol and a thin microscope slide. Dry nitrogen gas channeled into the space above the lens surface (through a circular glass apparatus) was used to prevent condensation. The laser microprobe system (Fig. 1) consists of (*i*) a modified Zeiss microscope with a video camera to aid in composing and focusing the image, (*ii*) a sample stage with x–y actuators, (*iii*) a triple monochromator [filter stage: two 150 grooves per mm of grating in antiparallel substractive configuration; spectrograph stage: three changeable gratings (150, 300, or 600 grooves per mm) for various spectral resolution], (*iv*) a 700-channel detector (Princeton Applied Research model 1420 intensified Reticon) cooled by Peltier elements, (*v*) a microcomputer (IBM XT) with laboratory-built interface boards for controlling the detector, an electronic shutter, and the x–y actuators, and (*vi*) laser sources (He/Cd, Ar^+, or Kr^+). To achieve flexibility, sensitivity, and high resolution (both spatial and spectral) for Raman scattering and fluorescence spectroscopy, we focus the laser beam to a point focus (1–8 μm) rather than a line and to move the sample under the microscope objective instead of deflecting the laser spot over the field of view of the microscope.

The excitation wavelength used was the 441.6-nm line from a He/Cd laser, and the concentration of the green fluorophor was measured by the fluorescence intensity at 520 nm (emission peak). A typical laser-scanning path covering the lens section is shown in Fig. 2. The scanning domain was 6.561 × 9.185 mm for the 5-month-old lens and 6.561 × 9.842 mm for the 73-year-old lens. The optical axis length and equatorial diameter for the 5-month-old lens were 4.1 mm and 6.4 mm, and for the 73-year-old lens were 4.2 mm and 8.6 mm, respectively. A total of 1200 data points was obtained in each experiment. This affords a high degree of spatial discrimination.

All the lens specimens were obtained from the Atlanta Lions eye bank. They were frozen at once in an aluminum block after removal from the eyes.

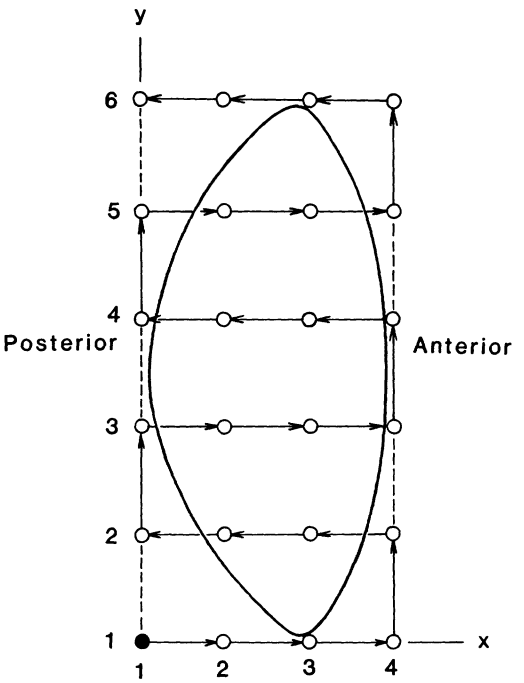

FIG. 2. Laser-scanning path on a lens section confined in a rectangular domain (≈ 6.5 × 9.5 mm). The lens section is along the optical axis and is perpendicular to the equatorial plane. Although 4 × 6 gridded points are shown, a total of 30 × 40 points are scanned in actual experiments. The solid point (1,1) is defined as the "home position" where scanning begins.

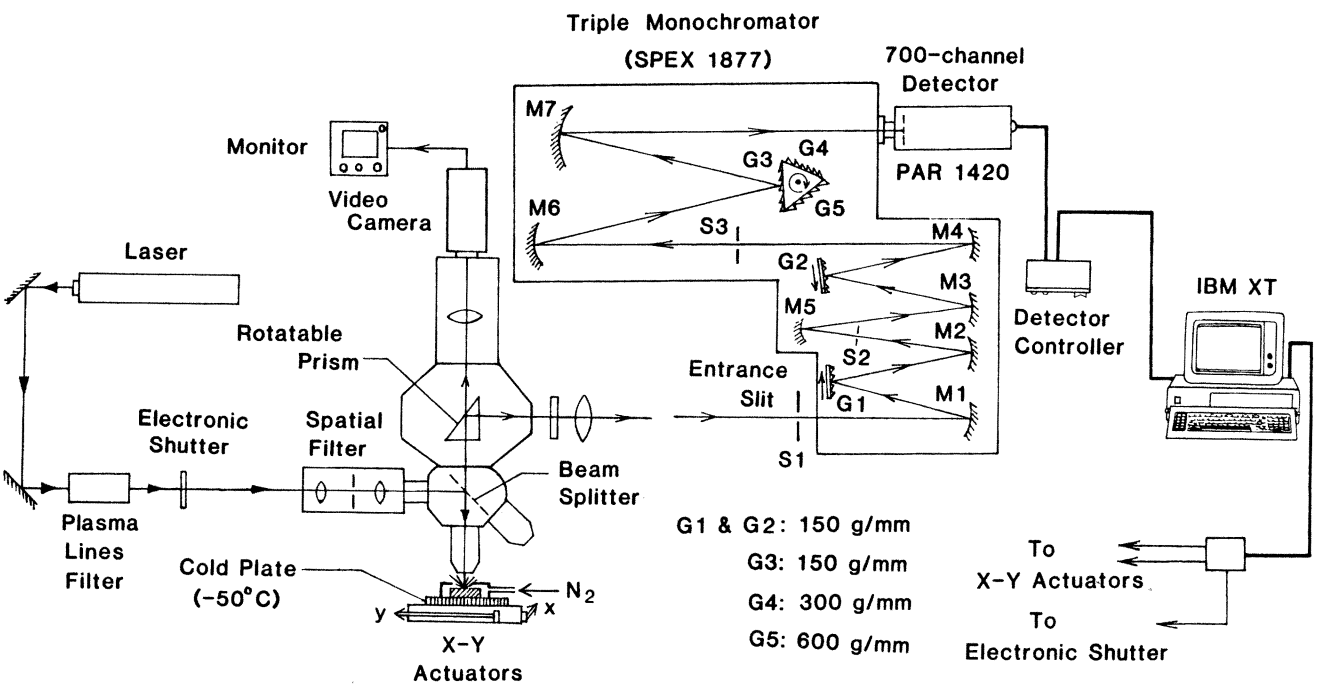

FIG. 1. Schematic diagram of the automated laser microprobe fluorescence/Raman scanning system. G1–G5, gratings; M1–M7, mirrors; S1–S3, slits.

RESULTS AND DISCUSSION

The green fluorophor distribution patterns for a 5-month-old lens (Fig. 3 *Left*) and a 73-year-old lens (Fig. 3 *Right*) are compared. The three-dimensional perspective profile for the young lens displays a cone-shape with its maximum near the lens center (Fig. 3*A*), whereas that of the old lens exhibits a distinct saddle shape: a plateau with a depressed central region and two unequal hill-like maxima near the equatorial cortical regions (Fig. 3*F*). Interestingly, there appears a strip of minor local maximum lying along the equatorial axis within the depressed inner region. The three-dimensional perspectives with cursor sectioning along the optical axis (Fig. 3 *B* and *G*) and along the equatorial axis (*C* and *H*) are also shown. The one-dimensional profile along the optical axis agrees well with that measured in *in vivo* on human patients, using the same laser excitation wavelength (13). Jacobs and Krohn (14) studied a similar fluorophor (emission maximum

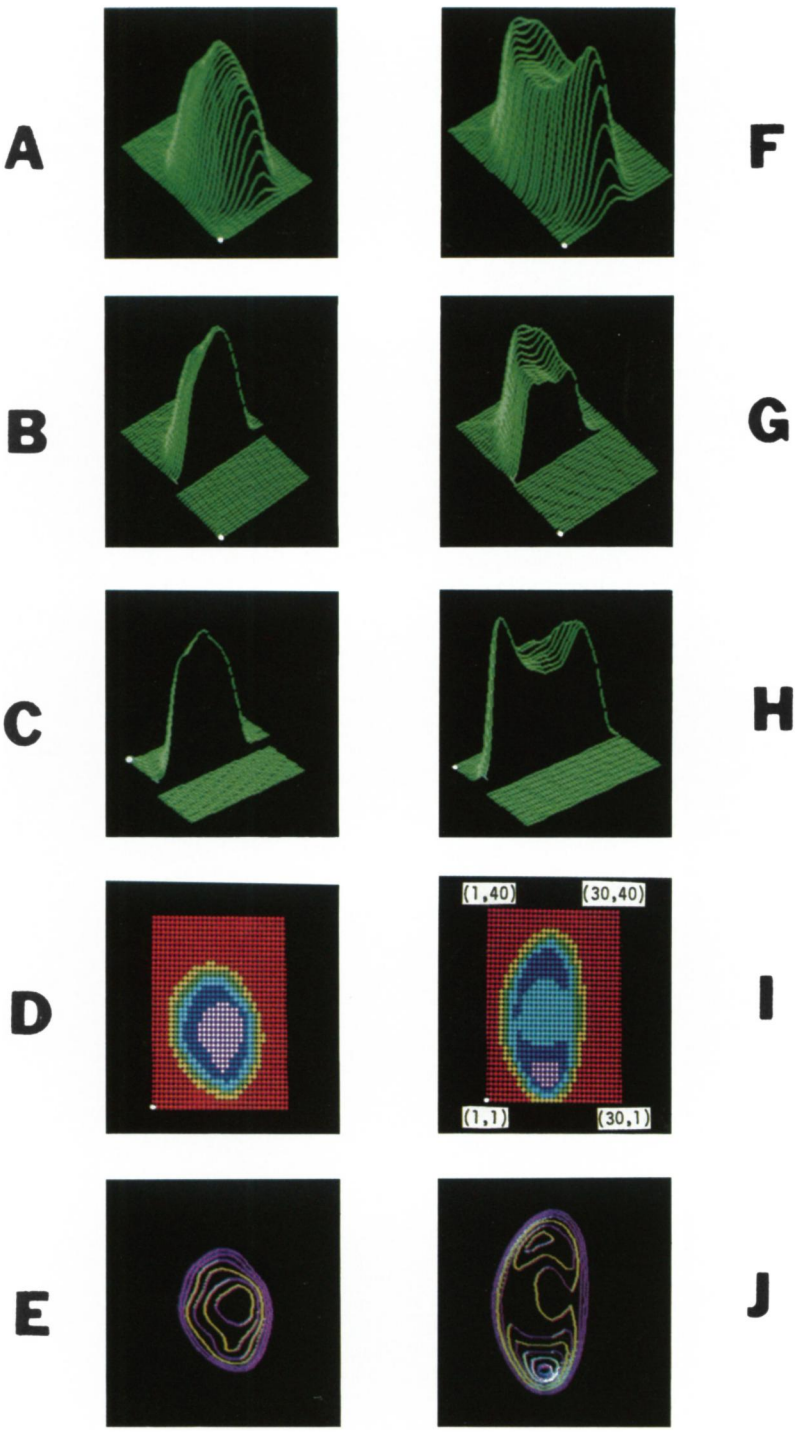

FIG. 3. Comparison of precise distribution patterns of the green fluorophor in 5-month-old lens (*Left*) and 73-year-old lens (*Right*). (*A* and *F*) Three-dimensional perspective profiles (the vertical intensities in *A*, *B*, and *C* should be reduced by 10 times when compared with those in *F*, *G*, and *H*). (*B* and *G*) Perspectives with cursor section along the lens optical axis. (*C* and *H*) Perspectives with cursor section along the equatorial axis. (*D* and *I*) Six-color maps (purple > blue > cyan > green > yellow > red). (*E* and *J*) Topographic contour maps. The home position is shown as a large white dot.

≈520 nm with excitation at 410 nm from an incoherent source) on thin lens sections and obtained the fluorescence intensity profiles along the optical axis that also exhibit a depressed inner plateau. However, they were not able to resolve the central local maximum (see Fig. 3*G*). It was also reported (14) that the fluorescence intensity of the entire nuclear region increased with age; the value at nucleus center increased ≈13 times from the 7-year-old lens to the 73-year-old lens. Our present data indicate that the fluorescence intensity at the nucleus center increases ≈10 times from a 5-month-old lens (1489 counts) to a 73-year-old lens (15,155 counts). The maximum intensity for the 73-year-old lens is 24,985 counts.

More interesting is the profile along the equatorial axis in the 73-year-old lens (Fig. 3*H*), exhibiting a minimum in the center, instead of a maximum expected on the basis of the light theory. Thus, we conclude that this green fluorophor is not generated by photocatalyzed reactions; it is produced by metabolic processes. Use of the term green fluorophor should not be taken to imply that it is a pure substance of known structure; it may even be a family of closely related fluorophors.

The fluorophor distributions are also presented in terms of color maps and topographic contours (panels D, E, I, and J). In color maps the intensity range between maximum and minimum was divided into six equal intervals, and colors were assigned to represent intensities in the following order: purple > blue > cyan > green > yellow > red. In topographic contours a total of 14 contour lines were drawn connecting the data points with constant height planes. It is interesting to note that along the optical axis the peak intensity is in the posterior segment of the lens. If this green fluorophor were produced photocatalytically, the peak height should be anterior; since it is not, the mode of production must be purely metabolic. The possibilities may also be considered that light impinging on the anterior has a bleaching effect or that partial destruction of the fluorophor is mediated by substances diffusing in from aqueous humor or the epithelium that is situated only anteriorly and is very active metabolically.

In conclusion, we have demonstrated a technique and methodology for sorting out the precise geometric distribution profiles of various fluorophors from which one may determine if a certain fluorophor is generated by metabolic processes or by ambient light. In general, the number of fluorophors increases with age in the human lens (15). It is possible to probe for fluorophors in the lens with various excitation wavelengths (15). The distribution profiles of orange (emission peak/excitation wavelength = 591 nm/568 nm), near red (633 nm/568 nm), red (672 nm/647 nm), and far red (707 nm/676 nm) fluorophors should be of great interest because the levels of these fluorophors are characteristically elevated in older and brunescent lenses (15, 16).

This work was supported by Grants EY01746 and EY07006 to N.-T.Y. and EY00260 to J.F.R.K. from the National Eye Institute.

1. Yu, N.-T., DeNagel, D. C., Ho, D. J.-Y. & Kuck, J. F. R., Jr. (1987) in *Biological Applications of Raman Spectroscopy: Raman Spectra and the Conformations of Biological Macromolecules*, ed. Spiro, T. G. (Wiley, New York), Vol. 1, pp. 47–80.
2. Yu, N.-T. & Barron, B. C. (1986) in *Supramolecular Structure and Function*, ed. Pifat-Mrzljak, G. (Springer-Verlag, Berlin), pp. 104–128.
3. Van Heyningen, R. (1973) in *Ciba Foundation Symposium* (Assoc. Sci. Pub., New York), Vol. 19, pp. 151–171.
4. Bando, M., Nakajima, A. & Satoh, K. (1981) *J. Biochem.* **89,** 103–109.
5. Pirie, A. (1971) *Biochem. J.* **125,** 203–208.
6. Lerman, S. (1972) *Isr. J. Med. Sci.* **8,** 1583–1589.
7. Augusteyn, R. C. (1975) *Ophthalmic Res.* **7,** 217–224.
8. Borkman, R. F., Dalrymple, A. & Lerman, S. (1977) *Photochem. Photobiol.* **26,** 129–132.
9. Grover, D. & Zigman, S. (1972) *Exp. Eye Res.* **13,** 70–76.
10. Borkman, R. F. (1977) *Photochem. Photobiol.* **26,** 163–166.
11. Zigler, J. S., Jr., & Goosey, J. D. (1981) *Photochem. Photobiol.* **33,** 869–874.
12. Yu, N.-T., Bando, M. & Kuck, J. F. R., Jr. (1983) *Invest. Ophthalmol. Vis. Sci.* **24,** 1157–1161.
13. Haughton, J. F., Yu, N.-T. & Bursell, S.-E. (1987) *Invest. Ophthalmol. Vis. Sci. Suppl.* **28,** 89.
14. Jacobs, R. & Krohn, D. L. (1981) *Invest. Ophthalmol. Vis. Sci.* **20,** 117–120.
15. Yu, N.-T., Bando, M. & Kuck, J. F. R., Jr. (1985) *Invest. Ophthalmol. Vis. Sci.* **26,** 97–101.
16. Bando, M., Yu, N.-T. & Kuck, J. F. R., Jr. (1984) *Invest. Ophthalmol. Vis. Sci.* **25,** 581–585.